Chapter 5

Fluorescence lifetime analysis of nitrite reductase from A. xylosoxidans at the single molecule level reveals enzyme mechanism[†]

[†] Tabares LC, Kostrz D, Elmalk A, Andreoni A, Dennison C, Aartsma TJ, Canters GW (2011) Fluorescence Lifetime Analysis of Nitrite Reductase from Alcaligenes xylosoxidans at the Single-Molecule Level Reveals the Enzyme Mechanism. Chemistry-A European Journal 17:12015-12019

Summary: *Immobilized fluorescently labelled bacterial nitrite reductase (NiR) has been studied during steady-state turn-over by single molecule fluorescence life time imaging (FLIM) microscopy. Two populations of single NiR molecules can be distinguished experimentally exhibiting different turn-over rates. The relative size of the populations varies with substrate (nitrite) concentration. The two populations are tentatively connected with two enzymatic routes: the 'reduction first' and the 'binding first' pathway.*

5.1 Introduction

Copper containing nitrite reductase (NiR) is a key enzyme in the bacterial denitrification and therefore plays important role in the global nitrogen cycle [1, 2]. The mode of action of this enzyme is highly contentious[3]. Herein we report new evidence on the enzyme's mechanism obtained from single molecule fluorescence lifetime imaging (FLIM) studies. We find two populations of molecules which correspond to two distinct mechanisms for the conversion of NO_2^- to NO. To our knowledge this is the first example of the use of lifetime switching as a tool to study the activity of a redox enzyme at the single molecule level.

NiR is a homotrimer with two Cu atoms per monomer (see section 5.6, Appendix, Figure A3)[4]. A type-1 (T1) copper site acquires reducing equivalents (electrons) which are transferred to a type 2 (T2) copper site where NO_2^- is converted into NO ($NO_2^- + e^- + 2H^+ \rightarrow NO + 2\ H_2O$). The dispute about the mechanism of this enzyme revolves around whether NO_2^- binds to the T2 copper site only after the latter has received an electron from the T1 copper site ('reduction first' mechanism)[5-9], or whether the electron is transferred only after binding of NO_2^- ('binding first' mechanism)[10-15]. These 'ordered' mechanisms are based on the assumption that there is some form of communication between the two centers about their state of reduction or the status of the substrate binding [16]. Conversely it has been argued by Wijma et al. that the enzyme operates according to a random sequential mechanism by which either pathway is feasible, the preponderant route depending on parameters such as pH and nitrite concentration [17]. This mechanism has received further support later on from the work of Scrutton and co-workers [18].

Herein we report evidence from single molecule FLIM studies that sheds new light on the catalytic mechanism of NiRs. This method is based on a newly devised technique which allows the redox behavior of T1 copper-containing oxido-reductases to be monitored[19-22]. The enzyme is covalently labeled with a fluorescent molecule whose emission spectrum overlaps with the absorption spectrum of the T1copper site (section 5.6, Appendix, Figure A4). A reduced T1 copper site has no absorption in the visible region and fluorescence is

(partly) quenched through Förster resonant energy transfer (FRET) only when the site is oxidized. During turn-over the fluorescence changes reflect fluctuations in the redox state of the T1 copper site [19-23]. The application of this approach to the study of the electro-chemical behavior of electron transfer proteins has been recently reported in this journal [24].

In earlier studies on green NiR (gNiR, section 5.6, Appendix, Figure A4) from *Alcaligenes faecalis*-S6 the intensity distributions in the fluorescence time traces of single molecules during turn-over exhibited severe overlap between the intensity histograms of the ox and the red form, allowing only an autocorrelation analysis of the data [22]. In the present case we have used the blue NiR from *A. xylosoxidans* (bNiR, section 5.6, Appendix, Figure A4) whose T1 copper site exhibits a much more pronounced absorbance around 600 nm (when oxidized) responsible for the protein's blue color [25]. This allows for an enhanced contrast between the red and ox forms of the T1 copper site of NiR, permitting more advanced data analysis. Another difference to the earlier studies is that instead of monitoring variations in intensity we have monitoring the fluorescence life time of labeled single enzyme molecules. The advantage is that the life time is insensitive to intensity fluctuations due to instrumental instabilities [26]. Two enzyme populations turning-over at different rates can be distinguished. Combining this information with a waiting time analysis we conclude that the two populations likely reflect the existence of two pathways, which may well correspond to the 'reduction first' and 'binding first' mechanisms.

5.2 Materials and Methods

5.2.1 Protein labeling

K329C bNiR was labeled at the free thiol group of the introduced Cys residue whilst the wild type (WT) protein was labeled at the N-terminus using modified versions of published protocols [18;19]. WT bNiR was exchanged into 100 mM 4-(2-hydroxyethyl)piperazine-1-ethanesulfonic acid (Hepes) pH 8.3 and the protein was incubated with 0.25 equivalents of ATTO 647N succinimidyl ester (ATTO-TEC GmbH) for 30 min at 4 ºC. Prior to labeling K329C bNiR was incubated for 2 h at 4 °C with 25-equivalents of TCEP and desalted on a Superdex 200 10/300 GL column (GE Healthcare) equilibrated in 20 mM Tris pH 7.5 containing 200 mM NaCl. Following this procedure, which removed some of the glutathione bound to Cys329 (*vide infra*), the protein was exchanged into 100 mM potassium phosphate pH 7.5 and incubated with an excess (in this case the exact amount of dye used was less important as the labeling ratio was dependent upon the amount of glutathione that had been removed from Cys329) of ATTO 647N maleimide (ATTO-TEC GmbH) for 1 h at 4 °C. Free dye was removed by desalting on a PD10 column (GE

Healthcare) equilibrated in 100 mM potassium phosphate pH 7.5. Labeling ratios were determined using ε values of 150 $mM^{-1}cm^{-1}$ at 644 nm for ATTO 647N and 60 $mM^{-1}cm^{-1}$ at 280 nm per monomer for bNiR.

5.2.2 Determination of switching ratios

Fluorescence time course experiments were performed on a Cary Eclipse fluorimeter in 50 mM potassium phosphate pH 7.5 using excitation and emission wavelengths of 630 and 657 nm respectively. The labeled protein concentrations were 31 nM for WT and 48 nM for K329C bNiR. The fluorescence intensities corresponding to the proteins in which the T1 copper was present as either Cu(I) or Cu(II) were determined by reducing the protein with sodium ascorbate containing phenazine-ethosulfate (PES) (stock solution of 1 M ascorbate plus 50 μM PES) and oxidizing with potassium ferricyanide (0.5 M stock solution) respectively. The switching ratio is the difference between the maximum (fully reduced protein) and the minimum fluorescence intensity (fully oxidized sample) divided by the maximum value.

5.2.3 Sample separation of single molecule studies

ATTO 647N-labeled K329C bNiR was immobilized on a glass slide in high purity agarose IV (Sigma) with a gel point of 36 ± 1.5 °C using a previously described procedure with some modifications. Prior to agarose deposition, the glass slides were incubated overnight in 10 % TritonX and sonicated sequentially for 30 min in 10 % TritonX, acetone, 3 M potassium hydroxide and methanol. Between these sonication steps the cover slips were rinsed and sonicated for 5 min in deionised (MilliQ) water. Subsequently the glass slides were incubated for 15 min in a 3:1 mixture of hydrochloric acid and nitric acid, sonicated for an additional 30 min, extensively rinsed with deionised water and spin-dried at 6000 rpm for 25 sec. The agarose (1 %) was melted in 100 mM potassium phosphate pH 7.5 and cooled to 50 °C. ATTO 647N-labeled K329C bNiR was added to give a final labeled protein concentration of 0.3 nM (the labeled protein is stable at 50 °C). Catalase (100 μg/ml) was added to the agarose in order to prevent possible deactivation of the enzyme. 200 μl of enzyme-containing agarose was spin coated onto a cleaned glass slide at 2000 rpm for 10 sec yielding a thin layer of gel. The coated glass was rapidly put into a holder and covered with 1ml of 100 mM potassium phosphate pH 7.5. Reduction was achieved using 100 mM phosphate pH 7.5 containing 100 μg/ml catalase, sodium ascorbate (10 mM) and phenazine-ethosulfate (PES) (100 nM). Oxidation was achieved with 100 mM phosphate pH 7.5 containing 100 μg/ml catalase and either 1.5 mM potassium ferricyanide or 50 mM $NaNO_2$. Enzyme turnover was studied in the presence of 100 mM phosphate pH 7.5 containing 100 μg/ml catalase, sodium ascorbate (10 mM) and PES (100 nM) plus

$NaNO_2$ (measurements were made using 5 μM, 50 μM, 500 μM, 1 mM and 5 mM $NaNO_2$). Although diffusion of chemicals through the thin agarose layer is very fast, a minimum of 10 minutes was allowed for equilibration. A fresh sample was used for each condition and measured for no more than one hour before discarding. Even at the lowest concentration of $NaNO_2$ the change in substrate concentration during this time is less than 1%.

5.2.4 Single molecule setup

Single-molecule fluorescence measurements were performed with a home-built scanning confocal microscope with Time-Correlated Single-Photon Counting (TCSPC) capabilities. Excitation was achieved with a pulsed picosecond diode laser (PDL 800-B, PicoQuant GmbH) emitting at 639 nm with 40 MHz repetition rate. The excitation beam was coupled into a single-mode fiber, passed through a narrow band clean-up filter (LD01-640/8-25, Semrock) and reflected by a dichroic mirror (Z 532/633 M) to a high numerical aperture (NA) oil objective (100× oil, NA 1.4, Zeiss) and on the sample surface. The power density at the sample was 0.5-1 kWatt/cm^2. The emitted fluorescence was filtered with an emission filter (D 675/50 M) and imaged onto the active area of a single photon counting avalanche photodiode (Perkin-Elmer SPCM-AQR-14) using a +4.5 mm achromatic lens. The data acquisition was done by the TimeHarp 200 TCSPC PC-board (PicoQuant, GmbH) working in the Time-Tagged Time-Resolved Mode. Samples were mounted onto a Physik Instrumente P-517 nanopositioner. Controlling of all the equipment and data acquisition were performed using SymPhoTime software (PicoQuant, GmbH).

5.2.5 Data collection

Fluorescence lifetime images were taken by scanning a 15x15 μm area of the sample with a step size of 75 nm and a dwell time of 4 ms per point. To determine the fluorescence lifetimes of the reduced and oxidized states (Figures 1A and 1B), a photon decay histogram of the photons collected over the whole image was constructed (Figure 2). Deconvolution with the instrumental response function (IRF) and a fit to a mono-exponential decay was carried out by using the SymPhoTime software (PicoQuant GmbH). Fluorescence decay times of (3.67±0.01) ns and (1.14±0.01) ns were found for the enzyme in the fully reduced and fully oxidized state, respectively. For all other conditions a sum of two exponentials was needed to obtain a satisfactory fit, demonstrating that in all these cases the sample contained a mixture of reduced and oxidized enzyme molecules. Fits were performed with fixed values of τ_1=1.1 and τ_2=3.7 ns.

5.2.6 Data analysis

To generate the FLIM pictures the fluorescence decay observed for each pixel was fit to a double exponential decay with fixed τ_1 and τ_2 (τ_1=1.1 and τ_2=3.7 ns) and by using the maximum likelihood algorithm, as implemented by the SymPhoTime software. Each pixel was colored either blue or red depending on whether the resulting average lifetime was smaller or larger than 2.5 ns, respectively. Pixels with a signal strength of less than 20 photons were discarded to reduce noise. Thus, we see (Figure 1) mostly red spots in the presence of reducing agents and mostly blue spots in the presence of oxidizing agents, while under turn-over conditions the spots consist of a mixture of red and blue pixels. The latter observation is a clear indication that during the scanning of a particular spot the T1 Cu is cycling between the oxidized and reduced state. A minimum of 6 pictures deriving from at least two independent measurements and containing an average of 50 spots per picture were analyzed for each condition.

To obtain the probability distribution of P_{ox} (Figure 3) for a spot a circular area around the center of the spot with a 15-pixel diameter (1.125µm) was selected and P_{ox} was calculated by dividing the number of blue pixels by the total number of red and blue pixels. Pixels containing less than 20 photons were rejected. P_{ox} histograms were fitted to a double Gaussian distribution except for the completely reduced or oxidized samples that were fit to a single Gaussian.

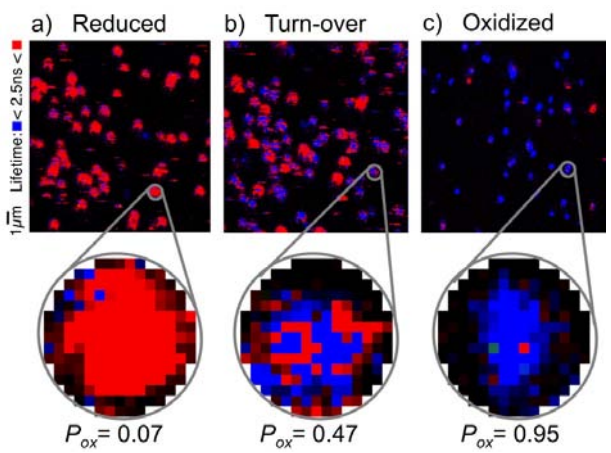

Figure 1. FLIM pictures of Atto647N-labelled bNIR-K329C immobilized in agarose gel. Top: in the presence of (a): 10mM ascorbate and 100 nM PES; (b): 10mM ascorbate,100 nM PES and 500 µM $NaNO_2$; and (c): 5 mM $NaNO_2$. Red and blue pixels correspond with fluorescence life times larger and smaller than 2.5 ns, respectively. Bottom: amplifications of selected spots.

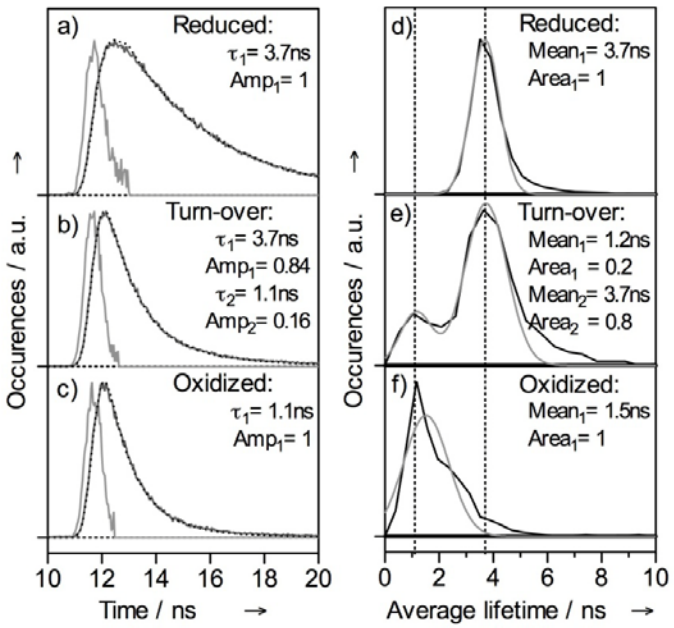

Figure 2. Fluorescence experiments on a sample of Atto647N-labelled bNIR-K329C immobilized in agarose gel. Data correspond to an area as depicted in Figure 1 containing ~40 spots. Left: Photon arrival time histograms for all photons present in one picture (dark lines) in the presence of (a):10mM ascorbate and 100 nM PES; (b): 10mM ascorbate,100 nM PES and 500 µM $NaNO_2$; (c): 5 mM $NaNO_2$. The gray line represents the instrument response function and dotted lines represent the fits to a single (a and c) or double exponential decay (b) (since fits follow very closely the experimental curves they may be difficult to distinguish in the figure). Fit results are given inside the picture. Right: Histogram of the photon life time per pixel for the same conditions as in the left panel (black line). The gray line presents the fit to a single (d and f) or double (e) Gaussian distribution (fit results are given in the picture).

5.3 Results

Figure 1, top, shows a 15x15 μm^2 area of a glass slide covered with a 300pM solid solution of Atto 647N-labelled NiR (NiR-A647N) in agarose, pH 7.5, at room temperature as observed under the fluorescence microscope. The size of the spots in Figure 1 is slightly larger (~600 nm full width at half maximum, FWHM) than the diffraction limit (~300 nm FWHM). The spots are scanned by small steps, each pixel in the image corresponding with a step size of 75 nm (Figure 1, bottom). The images were recorded under reducing (Figure 1a), oxidizing (Figure 1c) and turn-over (Figure 1b) conditions. Each spot corresponds with a single molecule of NiR that is singly labeled. The evidence for this derives from the

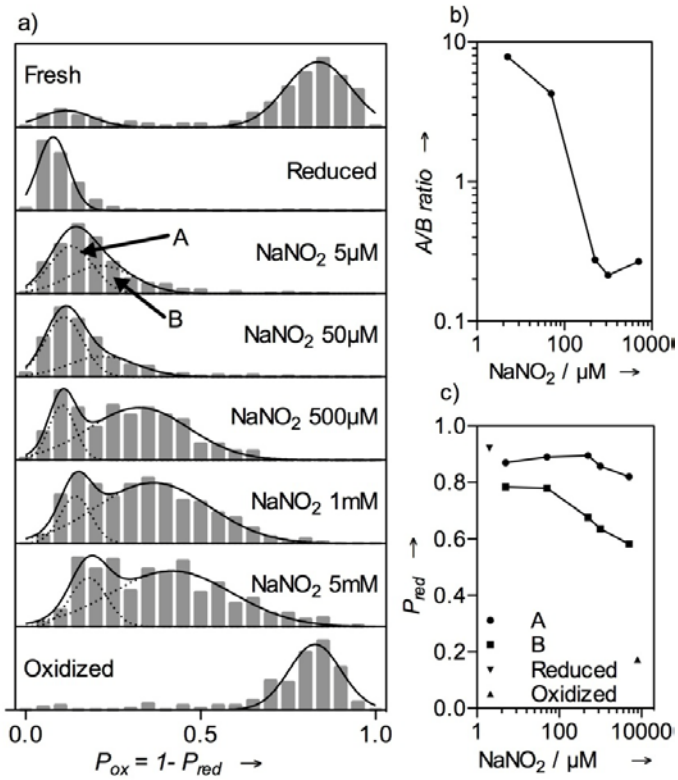

Figure 3. (a) Histograms of Pox observed under conditions as specified in the figure. For the panels labeled 'Fresh', 'Reduced' and 'Oxidized' the solid lines represent single Gaussian fits. In all other panels the fits (solid lines) are the sum of two Gaussian distributions (dotted lines). (b) Ratio between numbers of molecules in population A and population B during turn-over as a function of nitrite concentration. (c) Centers of the Gaussian distributions as function of nitrite concentration during turn-over. The values corresponding with completely reduced and completely oxidized enzyme are also shown.

bleaching behavior that every now and then is observed for a spot. Bleaching appears as a single step event by which the intensity is reduced to background levels.

Examples of fluorescence decay curves obtained by averaging over all the pixels in a 15×15 μm^2 area (see Figure 1) are presented in Figures 2a-2c together with the histogram of life times observed for the ensemble of pixels in the same area (Figures 2d-2e). The fluorescence decay times for the oxidized and reduced forms of NiR amount to (1.16±0.01) and (3.67±0.01) ns, respectively. This change corresponds with a FRET efficiency of 0.7 in good agreement with the 0.8 FRET efficiency observed for the bulk (see section 5.6,

Appendix). The pixels in the images of Figure 1 have been presented in false color, red and blue representing pixels for which the observed fluorescence life time is >2.5 ns or <2.5 ns, respectively. Thus, red corresponds with the reduced state and blue with the oxidized state. It is clear that under reducing (Figure 1a) or oxidizing (Figure 1c) conditions the enzyme molecules are overwhelmingly in the reduced or the oxidized state, respectively, while under turn-over conditions (Figure 1b) the redox state of the enzyme molecules alternates in time between reduced and oxidized during the scanning. The time-averaged degree of oxidation of a single spot, P_{ox}, ($P_{ox} = 1 - P_{red}$) was obtained by counting the number of blue pixels and dividing them by the sum of the blue and red pixels in the spot.

Figure 3a represents histograms of P_{ox} values for a few hundred spots as a function of the concentration of reductant and/or substrate (NO_2^-). As expected, under purely reducing or oxidizing conditions the distributions center at values of P_{ox} close to 0 or 1, respectively. Under turn-over conditions a much broader distribution of P_{ox} values is observed that can be decomposed into two populations, one (labeled A) that remains centered close to P_{ox} = 0, the other one (labeled B) that progressively moves towards larger values of P_{ox} as the concentration of substrate (NO_2^-) increases (see Figure 3c). At the same time the fraction of molecules in population A decreases with respect to population B (Figure 3b). Although

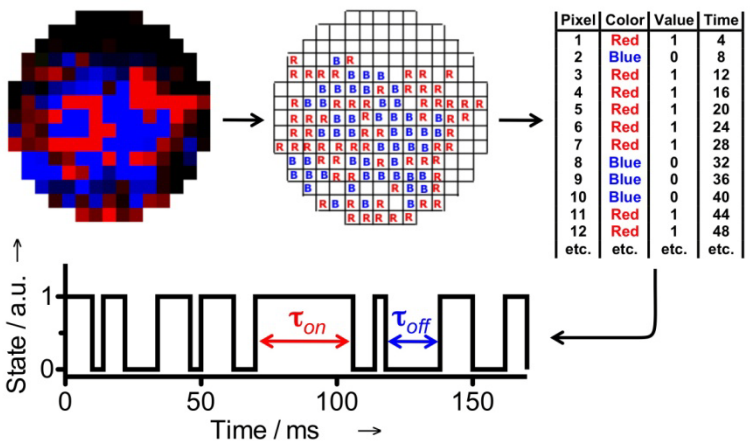

Figure 4. Analysis of the time dependent behaviour of a single enzyme molecule.The 75x75 nm pixels of the image (top, left) are scanned sequentially from top to bottom row by row, left to right, with a dwell time of 4 ms per pixel. A pixel is assigned a value of 0 or 1 depending on whether the fluorescence life time is < 2.5 ns (blue) or > 2.5 ns (red), respectively (top, middle). The values are collected in a table (top, right) whereby the pixels for which no signal could be read out due to a low intensity, were omitted. The pixel values were then plotted on a time axis (bottom) and waiting times (τ_{on} and τ_{off}) were read out.

the mean P_{ox} of population A or B under different turn-over conditions does not match the degree of oxidation encountered in-bulk under the same conditions, the overall weighted average, $[\sum P_{ox} \cdot n(P_{ox})]/ [\sum n(P_{ox})]$ does (Section 5.6, Appendix, Figure A6).

A waiting time analysis was performed by assigning a value of 1 or 0 to pixels, depending on whether the observed life time for a pixel was larger or smaller than 2.5 ns, respectively. The values were then pasted on a time axis each value taking a time interval of 4 ms (see Figure 4). Pixels for which no definite value for the fluorescence life time could be determined, for instance due to lack of sufficient photons, were omitted. Pixels in a row that did not correspond to the spot that was analyzed, were ignored. It was checked that the systematic error in the waiting time distributions introduced by this procedure was less than

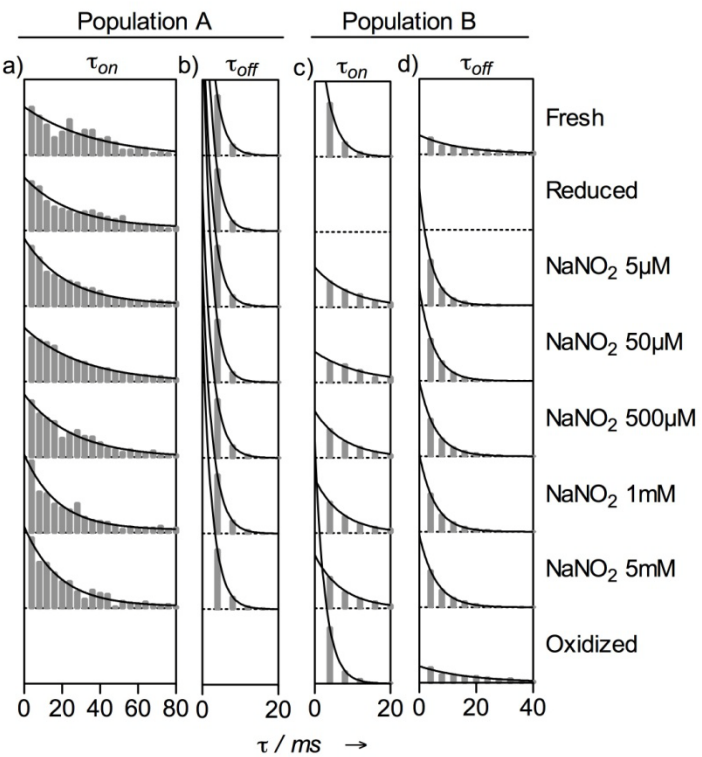

Figure 5. Histograms for the on (panels a and c) and off (panels b and d) times, τ_{on} and τ_{off}, for population A (a, b) and population B (c, d). To limit cross-contamination between the populations, for each condition the crossing point of the Gaussian fits was determined (P_c) and populations A and B were defined as the collections of spots with $P_{ox} \leq P_c - 0.025$ and $P_{ox} \geq P_c + 0.025$, respectively. The histograms are fit with single exponentials.

10% (see Appendix). Moreover it appeared that the results were not particularly sensitive to the detailed shape and size of the area that was used to define a spot (see Section 5.6, Appendix).

The on- and off-times (τ_{on} and τ_{off}) for a large number of spots were combined and used to construct histograms of τ_{on} and τ_{off} (see Figure 5). They could be fitted by single exponentials resulting in characteristic life times, τ_{red} and τ_{ox}, which denote the times during which the enzyme molecule stays in the reduced and the oxidized form, respectively. Values of τ_{red} and τ_{ox} as determined for different turn-over conditions are presented in Figure 6.

5.4 Discussion

As stated above, the data in Figure 3 point to the existence of two populations of NiR molecules. Molecules of population A exhibit an average degree of reduction close to 1 while the average degree of reduction of population B moves to lower values as the nitrite concentration increases. It is interesting to compare the waiting time distributions for the two populations.

Previously reported single molecule data on gNiR were analyzed with the customary three-state cyclic scheme depicted in Figure 7a [22]. In general, with a such a scheme, waiting time

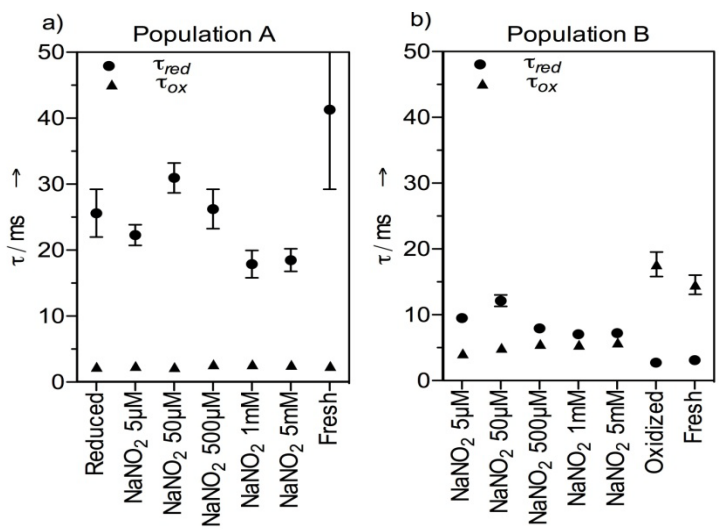

Figure 6. Life times in the reduced and the oxidized state (τ_{red} and τ_{ox}) for the populations A (panel a) and B (panel b) as determined from single exponential fits of the histograms of Figure 5. Error bars represent the standard error of the fit (in cases were error bars are not shown the standard error is smaller than the symbol size).

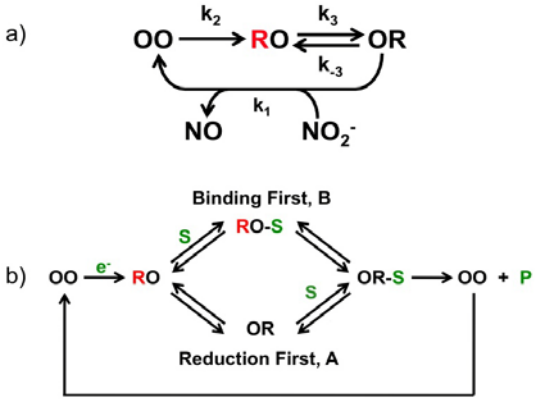

Figure 7. Scheme of the catalytic cycle of nitrite reductase. Scheme a represents the simple three-state cycle, in scheme b step 3 has been resolved in two steps leading to two alternative routes: the 'reduction first' route (route 'A') and the 'binding first' route (route 'B'). The symbols with the two capitals represent, from left to right, the T1- and the T2-sites, O and R denoting the oxidation state (oxidized and reduced, respectively). Red denotes the highly fluorescencing state. S denotes the substrate (NO_2^-) and P the product ($NO+H_2O$). The electron donor has been omitted for simplicity.

distributions are the sum of two exponentials [27]. In the present study however, bNiR FLIM data can be adequately fit with single exponentials (see Figure 5). This means that the faster decaying component is not resolved in our experiment where time resolution is limited by the dwell time per pixel of 4 ms and that we essentially monitor the reduction and oxidation of the T1copper site in time, *i.e.*, steps 2 and 3 according to the scheme in Figure 7a. During turn-over molecules in population A stay in the reduced state for about 20-30 ms while for population B this number is ~10 ms (see Figure 6). For both populations we observe that the waiting time for the next reduction step amounts to a few ms. For the resting state, on the other hand, the behavior is different (Figure 6; see data points denoted by 'Fresh', 'Oxidized' and 'Reduced'): molecules in population A spend longer times in the reduced form as compared to under turn-over conditions, while the opposite happens for population B, where molecules spend much longer times in the oxidized form.[‡] We note that the width of the distributions in Figure 3, in particular for population B, increases considerably when the nitrite concentration increases. This has

[‡] In the resting states, apparently, still some switching between the T1 redox states is observed possibly connected with intramolecular electron transfer between the T1- and the T2-sites.

been observed before for green-NiR and has been ascribed to a distribution in k_3, and may derive from structural disorder.

The enzyme kinetics of NiR in the bulk and in electrochemical experiments have been interpreted[17,28] on the basis of a scheme (Figure 7b) that distinguishes between the 'reduction first' and the 'binding first' pathway, which are labeled in Figure 7b by '*A*' and '*B*'. It is known from these experiments that at higher nitrite concentrations, and also at low pH, pathway '*B*' is favored over '*A*'. It is tempting to identify populations A and B with molecules that follow pathway '*A*' and pathway '*B*', respectively. Preliminary results show that the relative amount of molecules in populations A and B can be modulated by pH, indeed, in agreement with literature data on bulk solutions[17,28]. This would mean that electron transfer from the T1 to T2 copper site in molecules following path '*A*' is appreciably slower than in molecules that follow path '*B*' where nitrite is bound to the T2 copper site. This might be related to a change in driving force and/or in electronic coupling between the centers when nitrite binds. What causes a molecule to follow path '*A*' or '*B*'? Preliminary experiments seem to indicate that transitions from population A to population B are possible but occur at a relatively infrequent rate on the time scale of the present experiments (section 5.6, Appendix, Figure A7). This is the subject of ongoing research.

5.5 Conclusion

The present work confirms the random sequential character of the mechanism of NiR. The enzyme may follow the 'binding first' as well as the 'reduction first' pathway. The enzyme kinetics also exhibit features that are reminiscent of an ordered mechanism, in the sense that once an enzyme molecule operates according to path '*A*' or path '*B*', it keeps doing this at least for a number of turn-overs. The relatively low number of photons collected per spot before the label bleached necessitated the waiting times of large numbers of spots to be combined. Thereby a possible variation in τ_{on} and τ_{off} from spot to spot was averaged out. Future experiments will be aimed at obtaining improved signal/noise that would allow the observation of variations in rate from molecule to molecule.

5.6 Appendix

5.6.1 Site directed mutagenesis

The K329C mutation to the blue nitrite reductase (bNiR) from *Alcaligenes xylosoxidans* was created using QuikChange mutagenesis (Stratagene). The plasmid pET22b-bNiR [25] was used as the template along with the following primers; 5'-CTGATGAAGCA GATC**TGC**GCGCCCGCGCCGATTCC-3' (forward) and 5'-GGAATCGGCGCGGGC GC**GCA**GATCTGCTTCATCAG-3' (reverse). The sequences of both strands of the mutated plasmid (pET22b-bNiRK329C) were verified.

5.6.2 Over-expression, isolation and purification of the wild type and K329C bNiR

Wild type (WT) bNiR was over-expressed, isolated and purified as described previously [26]. For the K329C variant the only modification to this method was that the amount of streptomycin sulfate used for the precipitation of DNA during purification was lowered to 0.3 %. Purity was confirmed by sodium dodecyl sulfate polyacrylamide gel electrophoresis (12.5 % gel), with both WT and K329C bNiR having A_{280}/A_{594} ratios of around 11 for the fully oxidized forms. Protein concentrations were determined using a molar absorption coefficient (ε) of 5200 $M^{-1}cm^{-1}$ at 594 nm [28].

5.6.3 Protein characterization

Gel filtration and matrix assisted laser absorption ionization time-of-flight mass spectrometry (MALDI-TOF-MS) studies were performed as described previously[24, 29] in 20 mM Tris pH 7.5 containing 200 mM NaCL and 40 mM Tris pH 7.5 respectively. MALDI-TOF-MS was also performed on a K329C sample and had been incubated with 300 equivalents of tris(2-carboxyethyl) phosphine hydrochloride (TCEP) for 1 h at room temperature. UV/vis spectra of oxidized WT and K329C bNiR were acquired at room temperature on a Perkin-Elmer λ35 spectrophotometer in 20 mM 2-(N-morpholino)-ethanesulfonic acid (Mes) pH 6.0 X-band EPR spectra of oxidized WT and K329C bNiR were acquired on a Bruker EMX EPR spectrometer at 80 K. protein sample for EPR were exchanged by ultrafiltration into 40 mM Tris pH7.5, concentrated and glycerol was add to the final concentration of 40 % (final Tris concentration of 24 mM). diphenylpicylhydrazyl (DPPH) and α,γ-bis-diphenylene-β-phenyl allyl (BDPA) were used as external reference compounds.

The elution volume of the K329C bNiR variant on the gel filtration column (73.9 ml) corresponds to a molecular weight (MW) of 114.3 kDa indicative of the protein being a

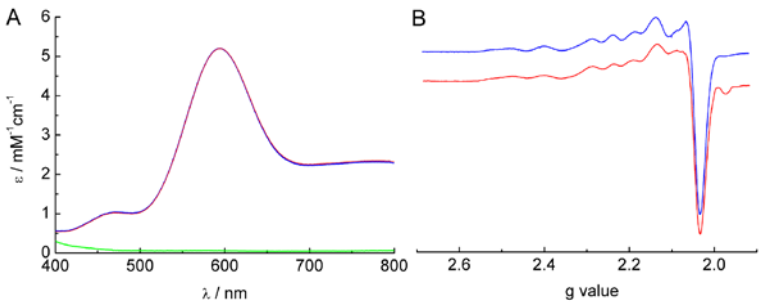

Figure **A1.** UV/Vis (A) and X- band EPR (B) spectra of oxidized WT (blue lines) and oxidized K329C (red lines) bNiR. The optical spectra of both species coincide. The spectra of both reduced species also coincide (green line). The UV/Vis spectra (room temperature) are obtained in 20 mM Mes pH 6.0 whilst EPR spectra (~ 80 K) are of samples in 24 mM Tris pH 7.6 (40 % glycerol).

stable trimer in solution, which is also the case for the WT protein (elution volume of 73.8 ml corresponding to a MW of 115.2 kDa). MALDI-TOF-MS gives a molecular weight of 36928.0 for the K329C bNiR monomer, which is 298.25 Da heavier than the theoretical value (36629.75 Da). This mass difference indicates that a small molecule, most likely glutathione (MW = 307.3 Da), attaches to the mutated protein via the introduced Cys residue during over-expression in the cytosol of *Escherichia coli*. Consistent with this, K329C bNiR reduced with TCEP gives a MW of 36618.4, very close to the theoretical value. The UV/Vis and EPR spectra of WT and K329C bNiR are very similar (See section 5.6, Appendix, Figure A1) and therefore this mutation has no effect on the structure of either the T1 or T2 copper sites. Furthermore, the removal of glutathione with TCEP did not influence the spectral properties of the variant.

The fluorescence switching ratios are almost identical for WT and K329C bNiR (0.86 and 0.84, respectively; see section 5.6, Appendix, Figure A2), which are labeled at the N-terminus and Cys329 respectively. The single molecule experiments described in this study were performed with the K329C variant as labeling via a Cys residue is more specific. Furthermore, the location for the introduced Cys residue was chosen so that the distance between the label and the T1 copper site within the same monomer was optimal for FRET whilst limiting the influence of redox changes at the two other T1 copper sites in the trimer. This is also ensured by maintaining a low labeling ratio (~11 % for the 'in bulk' experiments with WT and ~13 % for the K329C mutant samples used for 'in bulk' and the single molecule measurements).

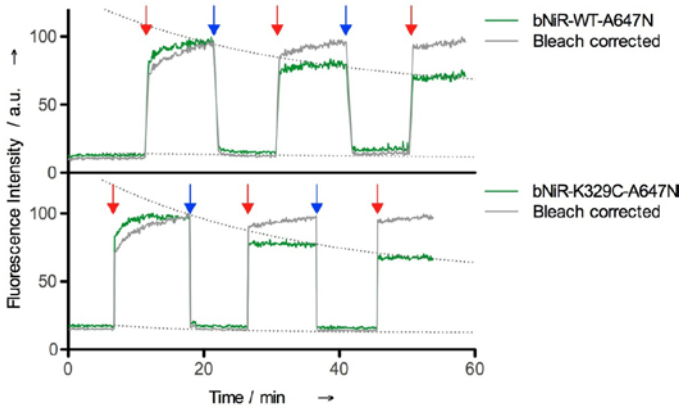

Figure A2. Fluorescence intensity changes upon reduction and oxidation of ATTO 647N-labeled WT (top) and K329C (bottom) bNiR. The labeled protein concentrations are 31 and 48 nm respectively with the samples in 50 mm phosphate pH 7.5. The arrows indicate the addition of (red) an excess of reductant (sodium ascorbate plus PES) and (blue) oxidant (potassium ferricyanide). The fluorescence intensity changes were followed at 657 nm using an excitation wavelength of 630 nm. The green trace is the experimental trace. It is known that the ATTO 647N dye under illumination may bleach in time. The manufacturer provides an example with a time constant of 28 min which was used here (dotted lines). When corrected for this (grey traces) the slow intensity decay with time disappears.

Figure A3. Structure of bNiR showing the entrance of the electron through the T1 Cu, the subsequent transfer of the electron to the T2 Cu and the conversion of NO_2^- into NO at the T2 Cu site. A dye molecule at position K329 is shown in purple. The reductant that reduces the T1-site is symbolized by X.

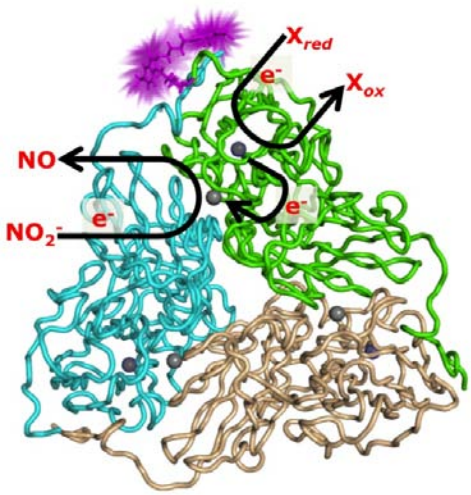

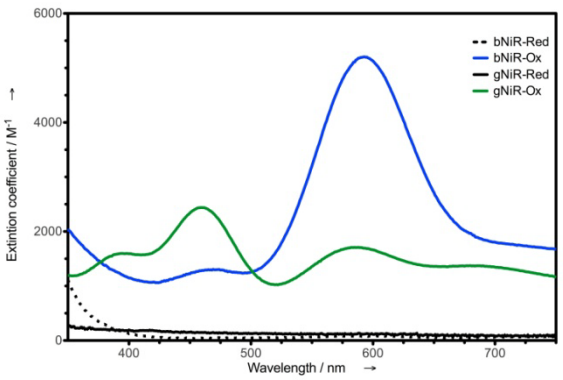

Figure A4. The visible absorption spectra of blue-NiR (bNiR) and green-NiR (gNiR) in the reduced (Red) and the oxidized (Ox) states.

5.6.4 Waiting time histograms

Waiting time histograms were constructed as described in the main text. We note that the data were obtained from a 15x15 µm surface area that was scanned row by row. This means that of all the pixels recorded for a single spot only the pixels in one row are contiguous in time, *i.e.*, there is an interval of about 0.8 sec between the data points in two consecutive rows (0.8 sec is the time needed by the scanner to scan a full line: 200 pixels of 4 ms each). We have disregarded the 0.8 sec time intervals between subsequent rows and treated the remaining pixels for one spot as a continuous series of time points. To check if this would introduce any major an On/Off trace was simulated by generating a 6×10^6 row of data-points $y(x)$ in which x is the time and y = 1 or 0. The x-axis was divided in increments of 1×0^{-5} sec mimicking a 60 s long trajectory with 0.01 ms resolution. At x = 0, y was arbitrarily set to "On" ($y=1$), followed by one "Off"-period ($y=0$) before another On-period was started. While Off-periods were fixed to 1000 points (τ_{off} = 10 ms), the On-periods were allowed to last for a time $\tau_{on} = -1 \times \ln(rand) \times \tau_{red}$, where *rand* is a computer-generated evenly-distributed random number between 0-1. In this way the On-periods lasted for a random time τ_{on}, the cumulative distribution of which obeys an exponential decay with time constant τ_{red}. Traces were generated in this way for τ_{red} = 0.5, 1, 3, 5, 10, 25, 50, 100 or 200 ms. These On/Off traces were then binned with bin sizes of 1 or 4 ms and histograms for τ_{on} were constructed (Figure A5).

To account for the non-contiguous character of the experimental time series the 60 s, 4ms-binned simulated-trace was treated as in the spot measurements, *i.e.*, blocks were extracted separated by intervals of 800 ms. The latter periods were discarded. The extracted blocks

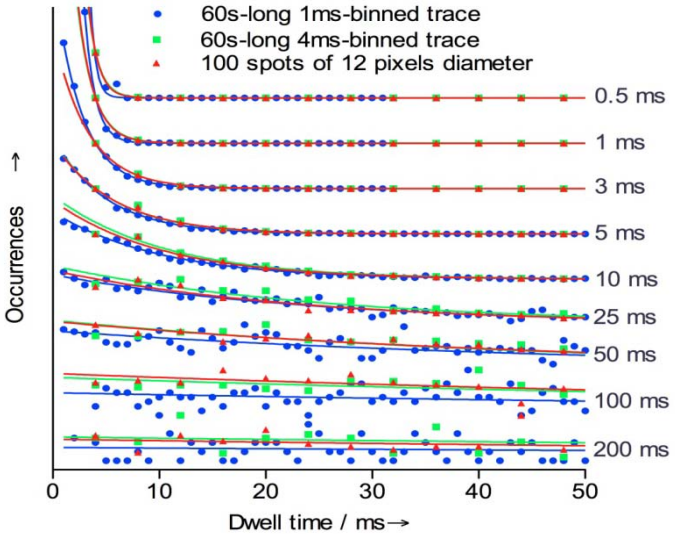

Figure A5. Dwell time histogram for the On-state of simulated time traces using different red values as specified at the right side of the picture (see text for details). Lines show the fit to a simple exponential decay

had subsequent lengths of 20 ms, 36 ms, 44 ms, 52 ms, 52 ms, 52 ms, 52 ms, 52 ms, 44 ms, 36 ms, 20 ms. This pattern corresponds with a circular spot with a 12 pixel diameter. The extracted blocks were placed one behind the other to form a continuous time trace. For each τ_{red} 100 independent traces were generated to mimic 100 spots, the time traces of which were analysed in the same way as the experimental data. The simulated data were used to construct dwell time histograms as presented in Figure A5. They were fitted with single exponentials, the exponential decay constants providing estimates of τ_{red}. Apart from the procedure described above to construct and analyze spots, we also analyzed the full 60 sec trajectories, not only with 4 ms bins but also with 1 ms binning. The results are summarized in Table A1. A less extensive simulation mimicking only 50 spots of 5 pixel diameter produced results that did not deviate from the 4 ms continuous traces by more than 30%.

As can be seen from Table A1, the effect of bin size on the extracted time constant becomes noticeable only towards shorter time constants where τ_{red} is of the order of or smaller than the bin size. More importantly, the procedure of chopping up the time trace - as done in this study - for analyzing the experimental data, does not seem to introduce appreciable errors. Apart from the small error that may be introduced, the attractive feature

Theoretical τ_{red} (ms)	60s-long 1ms-binned trace		60s-long 4ms-binned trace		100 spots of 12 pixels diameter; bin size 4 ms	
	Fit τ (ms)	Abs. error (%)	Fit τ (ms)	Abs. error (%)	Fit τ (ms)	Abs. error (%)
0.5	0.5	1	1.0	95	0.9	82
1	1.0	2	1.5	52	1.5	46
2.5	2.6	2	3.2	28	3.2	28
5	5.0	1	5.6	12	5.7	14
10	10.2	2	10.5	5	10.3	3
25	25	1	27	2	24	4
50	52	3	47	7	50	1
100	112	12	108	8	102	2
200	198	1	178	11	137	32

Table A1. Results of fitting of dwell time histograms of presented in figure A5 to a single exponential decay. The table shows results of decay times (τ) for the dwell time histograms of traces simulated with τ_{red} values of 0.5, 1, 3, 5, 10, 25, 50, 100 or 200 ms (see text). The errors represent the absolute (Abs.) error of the fitted decay when compared to the theoretical value of the simulation.

of the procedure followed here is that with a 10 minutes measurement (which does not involve selection of individual molecules) and a computational procedure that proves to be fast, it is possible to identify the state (oxidized, reduced or turning over) of every molecule together with its kinetics parameters. The use of lifetime over intensity also eliminates background effects and artifacts introduced by dye blinking.

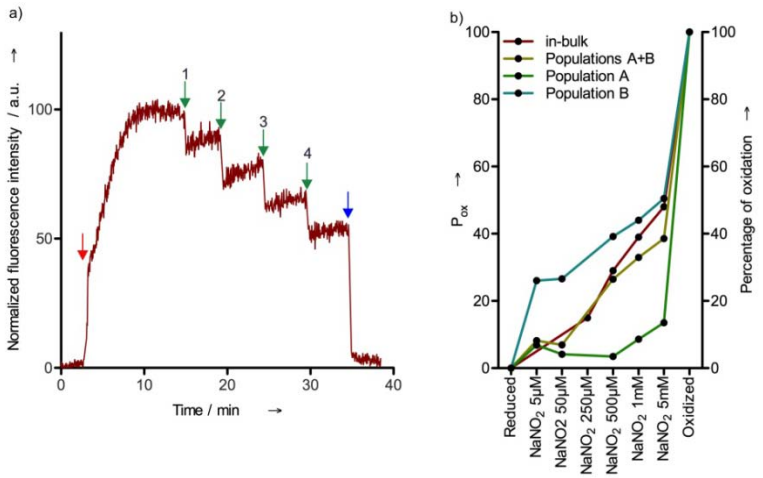

Figure A6. Left: Normalized in-bulk fluorescence intensity time trace of bNiR-Atto647N, corrected for bleaching (see Figure A2). The arrows indicate the addition of reductant (red; 10 mM sodium ascorbate plus 100 nM PES), $NaNO_2$ (green: 1, 250 µM; 2, 500 µM; 3, 1000 µM and 4, 5000 µM, final concentrations) and oxidant (blue; 20 mM $K_3Fe(CN)_6$). **Right:** Comparison of mean P_{ox} for population A, B and A+B with the in-bulk percentage of oxidation calculated from the left panel. The data was normalized between 0 and 100.

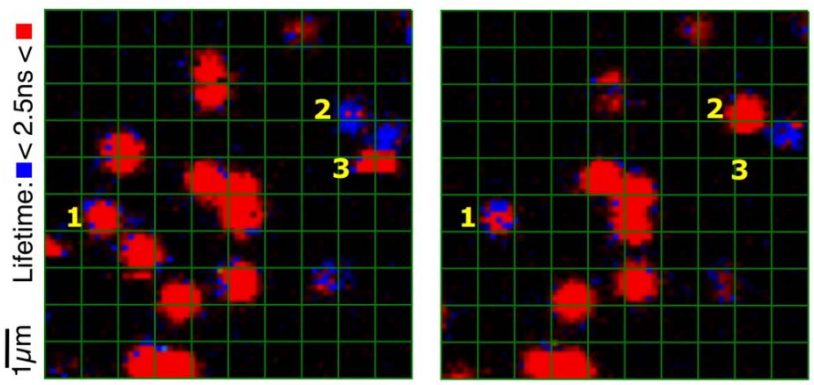

Figure A7. Example of switching between populations. The two images were taken of the same area under the same conditions with an interval of 10 min (left first). Molecule 1 switches from population A to B while the opposite happens to molecule 2. The green grid (1×1 µm) helps to compare the position of the molecules. A few molecules disappear when going from the left image to the right due to bleaching. In the left image a single-step photo-bleaching can be observed during the scan for molecule 3.

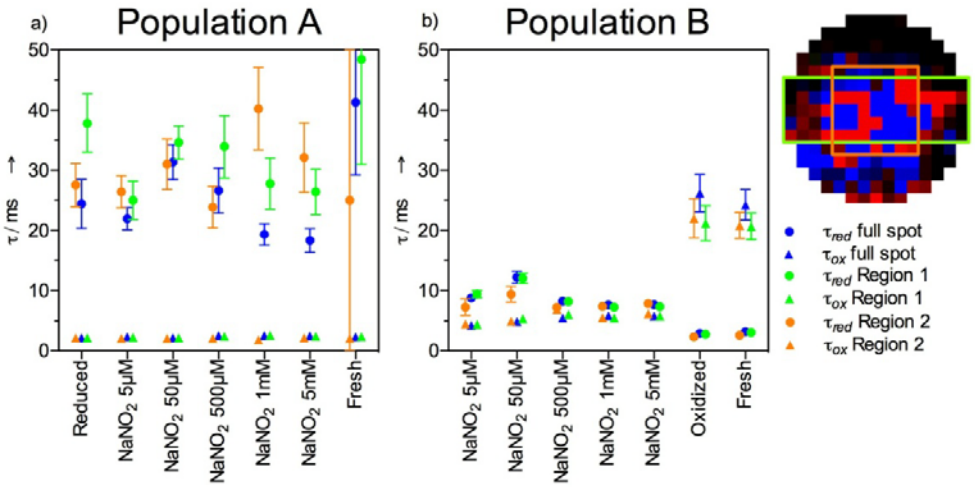

Figure A8. Effect of selected spot area on the values of τ_{red} and τ_{ox} as obtained for the populations A (panel a) and B (panel b). Blue points: data obtained by analyzing all the pixels within a spot with a diameter of 15 pixels. Orange points: data obtained by analyzing all the pixels within a square of 7×7 pixels around the center of the spot; green points: data obtained by analyzing all the pixels within an area of 5×15 pixels around the center of the spot. The different areas and the corresponding spots are presented at the right of the figure. The spot depicted in Figure 4 was used above for illustrative purposes.

References

1. Ferguson SJ. Nitrogen cycle enzymology. **1998,** *2* 182-193.
2. Zumft WG. Cell biology and molecular basis of denitrification. *Microbiol. Mol. Biol. Rev.* **1997,** *61* 533-616.
3. Ghosh S. Spectroscopic and Computational Studies of Nitrite Reductase: Proton Induced Electron Transfer and Backbonding Contributions to Reactivity. *J. Am. Chem. Soc.* **2009,** *131* 277-288.
4. Adman ET and Murphy MEP in Handbook of Metalloproteins, Vol. 2 (Eds. : A. Messerschmidt, R. Huber, T. Poulos, K. Wieghardt), Wiley, New York, 2001, pp. 1381 –1390.
5. Abraham ZHL. pH-dependence for binding a single nitrite ion to each type-2 copper centre in the copper-containing nitrite reductase of Alcaligenes xylosoxidans. *Biochem. J.* **1997,** *324* 511-516.
6. Jackson MA. Evidence for An No-Rebound Mechanism for Production of N2O from Nitrite by the Copper-Containing Nitrite Reductase from Achromobacter-Cycloclastes. *Febs Lett.* **1991,** *291* 41-44.
7. Averill BA. Dissimilatory nitrite and nitric oxide reductases. *Chem. Rev.***1996,** *96* 2951-2964.
8. Hulse CL. Evidence for A Copper Nitrosyl Intermediate in Denitrification by the Copper-Containing Nitrite Reductase of Achromobacter-Cycloclastes. *J. Am. Chem. Soc.* **1989,** *111* 2322-2323.
9. Wasser IM. Nitric oxide in biological denitrification: Fe/Cu metalloenzyme and metal complex NOx redox chemistry. *Chem. Rev.* **2002,** *102* 1201-1234.
10. Suzuki S. Metal coordination and mechanism of multicopper nitrite reductase. *Acc. Chem. Res.* **2000,** *33* 728-735.
11. Murphy MEP. Structure of nitrite bound to copper-containing nitrite reductase from Alcaligenes faecalis - Mechanistic implications. *J. Biol. Chem.* **1997,** *272* 28455-28460.
12. Adman ET. The Structure of Copper-Nitrite Reductase from Achromobacter Cycloclastes at 5 Ph Values, with No2- Bound and with Type-Ii Copper Depleted. *J. Biol. Chem.* **1995,** *270* 27458-27474.
13. Kataoka K. Functional analysis of conserved aspartate and histidine residues located around the type 2 copper site of copper-containing nitrite reductase. *J. Biochem.* **2000,** *127* 345-350.
14. Boulanger MJ. Catalytic roles for two water bridged residues (Asp-98 and His-255) in the active site of copper-containing nitrite reductase. *J. Biol. Chem.* **2000,** *275* 23957-23964.
15. Hough MA. Crystallography with online optical and X-ray absorption spectroscopies demonstrates an ordered mechanism in copper nitrite reductase. *J. Mol. Biol.* **2008,** *378* 353-361.
16. Strange RW. Structural and kinetic evidence for an ordered mechanism of copper nitrite reductase. *J. Mol. Biol.* **1999,** *287* 1001-1009.
17. Wijma HJ. A random-sequential mechanism for nitrite binding and active site reduction in copper-containing nitrite reductase. *J. Biol. Chem.* **2006,** *281* 16340-16346.
18. Brenner S. Demonstration of Proton-coupled Electron Transfer in the Copper-containing Nitrite Reductases. *J. Biol. Chem.* **2009,** *284* 25973-25983.
19. Schmauder R. Sensitive detection of the redox state of copper proteins using fluorescence. *J. Biol. Inorg. Chem.* **2005,** *10* 683-687.

20. Kuznetsova S, Zauner G, Schmauder R, Mayboroda OA, Deelder AM, Aartsma TJ, Canters GW. A Forster-resonance-energy transfer-based method for fluorescence detection of the protein redox state. *Anal. Biochem.* **2006,** *350* 52-60.

21. Schmauder R. The oxidation state of a protein observed molecule-by-molecule. *ChemPhysChem* **2005,** *6* 1381-1386.

22. Kuznetsova S, Zauner G, Aartsma TJ, Engelkamp H, Hatzakis N, Rowan AE, Nolte RJM, Christianen PCM, Canters GW. The enzyme mechanism of nitrite reductase studied at single-molecule level. *Proc. Natl. Acad. Sci. U. S. A.* **2008,** *105* 3250-3255.

23. Davis JJ, Burgess H, Zauner G, Kuznetsova S, Salverda J, Aartsma T, Canters GW. Monitoring interfacial bioelectrochemistry using a FRET switch. *J. Phys. Chem. B* **2006,** *110* 20649-20654.

24. Salverda TM, Patil AV, Mizzon G, Kuznetsova S, Zauner G, Akkilic N, Canters GW, Davis JJ, Heering HA, Aartsma TJ. Fluorescent Cyclic Voltammetry of Immobilized Azurin: Direct Observation of Thermodynamic and Kinetic Heterogeneity. *Angew. Chem., Int. Ed.* **2010,** *49* 5776-5779.

25. Sato K and Dennison C.. Active site comparison of Co-II blue and green nitrite reductases. *Chem.-Eur. J.* **2006,** *12* 6647-6659.

26. Sorokina M. Fluorescent Lifetime Trajectories of a Single Fluorophore Reveal Reaction Intermediates During Transcription Initiation. *Chem. Phys.* **1999,** *247* 11-22.

27. Qian H and Elson EL.. Single-molecule enzymology: stochastic Michaelis-Menten kinetics. *Biophys. Chem.* **2002** *102-102* 565-576.

28. Wijma HJ, Jeuken LJC, Verbeet MP, Armstrong FA, Canters GW. Protein film voltammetry of copper-containing nitrite reductase reveals reversible inactivation. *J. Am. Chem. Soc.* **2007,** *129* 8557-8565.

29. Sato K, Firbank SJ, Li C, Banfield MJ, Dennison C. The importance of the long type 1 copper-binding loop of nitrite reductase for structure and function. *Chem.-Eur. J.* **2006,** *14* 5820-5828.